Available online at www.sciencerepository.org

Science Repository

Research Article

Impact of Collimator on DaT-SPECT Imaging: Monte Carlo Simulation Study

Akihiko Takahashi[1*], Keita Funada[2], Kazuhiko Himuro[3], Shingo Baba[4] and Masayuki Sasaki[1]

[1]*Division of Medical Quantum Science, Department of Health Sciences, Kyushu University, Fukuoka, Japan*
[2]*Personal Radiation Monitoring Service Department, Chiyoda Technol Corporation, Japan*
[3]*Division of Radiology, Department of Medical Technology, Kyushu University Hospital, Fukuoka, Japan*
[4]*Department of Clinical Radiology, Kyushu University Hospital, Fukuoka, Japan*

ARTICLE INFO

Article history:
Received: 18 December, 2019
Accepted: 30 December, 2019
Published: 21 January, 2020

Keywords:
^{123}I-ioflupane
DaT-SPECT
point-spread
spatial resolution correction
monte carlo simulation

ABSTRACT

Aim: The purpose of this study was to assess the impact of the collimator in viewing the dopamine transporter, using ^{123}I ioflupane single-photon emission computed tomography (DaT-SPECT) images utilizing a Monte Carlo simulation.

Methods: For the purpose of this study, the Monte Carlo simulation of electrons and photons (MCEP)-SPECT was used. A numerical phantom was created from a real basal ganglia phantom and installed within the code. The specific binding ratios (SBRs) were 5.03 and 2.01 for the background concentration of 7.44 kBq/mL or 7.04 and 3.03 for a background concentration of 5.56 kBq/mL. The simulated images were evaluated using a recovery coefficient (RC). Initially, we simulated the performance of 14 collimators without resolution correction to investigate the impact of the collimator dimension. The effects of two resolution correction methods (collimator broad correction (CBC) and three-dimensional frequency–distance relationship (3D-FDR)) on two reconstruction methods (Ordered-Subsets Expectation Maximization (OSEM) and Filtered back projection (FBP)) was assessed for collimators that demonstrated a better RC value.

Results: Five low-energy high-resolution (LEHR) collimators and one medium-energy general-purpose (MEGP) collimator demonstrated superior RC values. These collimators had a high aspect ratio (hole-length/hole-diameter). The maximum RC value without resolution correction was 64.9% when the image was reconstructed with OSEM. The RC value improved to 79.7% when the resolution correction of CBC was applied. When the resolution collection was applied, the RCs improved by approximately 1.2 times when compared against those without the resolution correction. In terms of the reconstruction method, the RC obtained using OSEM was statistically insignificant when compared to the RC using FBP. The difference in the RC value with collimators decreased according to resolution correction.

Conclusion: The LEHR collimator with a high aspect ratio, and the OSEM with spatial resolution correction were confirmed to be appropriate for DaT-SPECT imaging. In terms of the reconstruction method, CBC was more favourable than FDR.

Introduction

The primary factor determining the quality of single-photon emission computed tomography (SPECT) images is the performance of the collimators. Poor collimators will lead to blurring at the border of the hot areas. The role of the collimators is, to block oblique-incidence photons. However, collimators have finite hole-diameters and lengths; as a result, they demonstrate distinct point-spread characteristics. In addition, the photons that penetrate the septa are scattered leading to spreading of the point source. These geometric and physical factors limit the spatial resolution and quality of a SPECT image [1]. The physical factors, penetration or scattering of photons in the collimator is dependent upon

[*]*Correspondence to: Akihiko Takahashi, Kyushu University, Maidashi 3-1-1 Higashi-ku, Fukuoka, Japan; Tel: +81926426725; Fax: +81926426674; E-mail: takahsr@hs.med.kyushu-u.ac.jp*

http://dx.doi.org/10.31487/j.RDI.2019.04.06

the septal thickness and photon energy; therefore, it should be difficult to assess the impact of the physical factor using a simple equation.

This study was designed assess the impact of the collimator on the image quality of SPECT images and the effect of the resolution correction method using a Monte Carlo simulation. The advantage of physical simulation is to consider various conditions of the target factors (collimators and resolution correction methods, etc.). However, in reality, the different types of collimators are limited, and several SPECT devices are used; therefore, the effect of various factors on each device should be investigated (e.g., performance of cameras or correction methods) [2]. In this study, we simulated the performance of 14 different collimators, two kinds of reconstruction methods, and two kind of resolution correction methods.

We adopted a dopamine transporter imaging with SPECT (DaT-SPECT) as the sample in this study. The DaT-SPECT has been used for the diagnosis of Parkinson's disease and dementia with Lewy bodies and the assessment of ^{123}I-ioflupane accumulation in the striatum [3-6]. Because the striatum is a small tissue and is deeply located, it can be easily affected by the deterioration of spatial resolution in the SPECT imaging test. Therefore, improvements in spatial resolution is important to quantify DaT images [7].

In order to accurately assess the effect of spatial resolution correction in DaT-SPECT, a collimator broad correction (CBC) and restoration-filtering based on three-dimensional frequency distance relationship (3D-FDR) were tested [1, 8, 9]. The CBC is used for ordered-subset expectation maximization (OSEM) to correct the deterioration of spatial resolution by inserting correction terms in the reconstruction algorism [8]. On the other hand, the 3D-FDR method is based on the Fourier transform of a sinogram, which is applied to projected data prior to reconstruction [10]. The 3D-FDR method, which is mainly used for filtered back projection (FBP), can be applied for OSEM [11]. Regarding DaT-SPECT imaging, improvements in image quality produced by spatial resolution correction using 3D-FDR has not been studied. In this study, the coupling effects of collimators and these resolution correction methods were also investigated.

Materials and Methods

I Simulation Code and Phantom

The Monte Carlo simulation in this study included in-house codes, namely the Monte Carlo simulation of electrons and photons (MCEP) and MCEP-SPECT [12, 13]. MCEP-SPECT is based on the gamma camera simulation codes HEXAGON and NAI developed by Tanaka et al. [14]. The HEXAGON and NAI were developed for ^{123}I scintigraphy, which correctly simulated the experimental results of ^{123}I spectra. (Figures 1 and 2) show the MCEP-SPECT schematic and the photo of basal ganglia phantom, respectively. The size of the collimator and NaI crystal was 40 cm × 40 cm. To simulate the effects of backscatter photons from the backward components (photomultiplier tubes), a glass and aluminum plate was placed behind NaI. A numerical phantom was created using computed tomography (CT) images of the real basal ganglia phantom (NMP Business Support Co., Ltd., Hyogo, Japan) and analyzed using MCEP-SPECT (Figure 2). The voxel size was 0.6 mm (width) × 0.6 mm (height) × 1 mm (length). The radioactivity concentration of the right striatum was set to 44.9 kBq/mL, and that of the left striatum was set to 22.4 kBq/mL. The radioactivity concentration of the background was set to 5.56 or 7.44 kBq/mL.

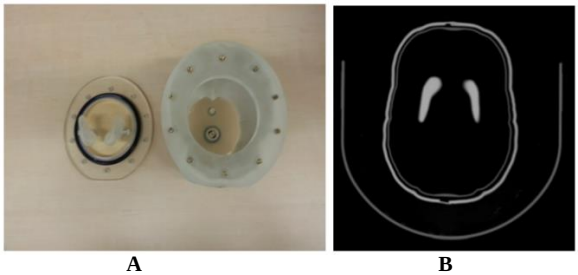

A B

Figure 1: A) Illustration of basal ganglia phantom. **B)** One of the CT images of the basal ganglia phantom.

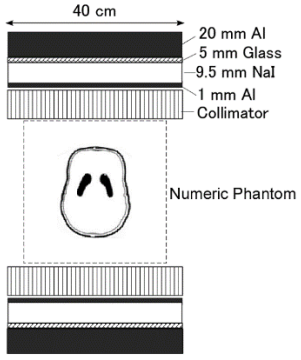

Figure 2: Setup for the simulation of SPECT imaging. The size of the numerical phantom was 30 cm (width) × 30 cm (height) × 26.5 cm (length), (512 pixels × 512 pixels × 256 slices).

The simulation settings were based on the imaging guidelines of DaT-SPECT and a previous study [15-17]. The main energy window was 143–175 keV (159 keV ± 20%). Furthermore, the acquisition time was 30 min and the number of projection images was 90 per 360 degrees. Radius of gyration of gamma cameras was 150 mm. The projection images were 128 pixels × 128 pixels, and the pixel size was 3.13 mm × 3.13 mm.

Table 1: Dimensions of collimators.

Collimator	Hole diameter (cm)	Septal thickness (cm)	Hole length (cm)	Aspect ratio*
LEHR-1	0.14	0.018	2.54	18
LEHR-2	0.14	0.018	2.7	19
LEHR-3	0.14	0.02	2.54	18
LEHR-4	0.14	0.025	2.54	18
LEHR-5	0.14	0.018	2.92	21
LEHR-6	0.157	0.025	2.54	16.2
LEGP-1	0.14	0.018	2.47	18
LEGP-2	0.178	0.025	2.54	14.3
LEGP-3	0.203	0.025	2.54	12.5
LEGP-4	0.229	0.025	2.54	11.1
LEGP-5	0.254	0.025	2.54	10.0
MEGP-1	0.17	0.02	3	18
MEGP-2	0.207	0.066	3.284	15.9
MEGP-3	0.25	0.12	3.5	14

*Aspect ratio = Hole length/Hole diameter.

II Collimators

The dimensions of parallel hexagonal collimator holes are listed in (Table 1). This data were based on "THE COLLIMATOR DATABASE", which is attached in the SIMIND Monte Carlo code. We investigated 14 collimators, including six low-energy, high-resolution (LEHR); five low-energy, general-purpose (LEGP); and three medium-energy, general-purpose (MEGP) collimators. Table 1 shows the aspect ratios, representing ratios of the hole length to the hole diameter.

III Image Reconstruction and Correction

To reconstruct and correct the SPECT images, we used the imaging software package for nuclear medicine: The Prominence Processor (version 3.1, distributed by the Prominence Conference, not for sale). The image reconstruction methods mainly included OSEM (iteration, 6; subset, 10) and FBP using a ramp filter. All SPECT images were commonly corrected via preprocessing, attenuation correction (AC), and scatter correction (SC). The preprocessing included the Butterworth filter (cutoff frequency: 0.5 cycles/cm, order: 8). Chang AC was used, with an attenuation coefficient of 0.146 cm^{-1}. For SC, triple-energy-window technique was used, with energy windows of 132-142 keV (137 keV ± 7.3%) and 176-186 keV (181 keV ± 5.5%).

IV Spatial Resolution Correction

To correct deterioration of spatial resolution, 3D-FDR and CBC were applied. 3D-FDR requires a spatial-frequency filter, the Metz filter, which is applied to the two-dimensional Fourier transformation of the sinogram prior to reconstruction. The Metz filter enhances a certain spatial-frequency component of the projection images, which corresponds to the outline of the hot area. The Metz filter is mathematically formulated as follows:

$$M(f) = MTF(f)^{-1}[1 - (1 - MTF(f)^2)^X] \quad [1]$$

where f is a spatial frequency, $MTF(f)$ is a modulation transfer function, and X is a noise-suppression parameter (*18*). According to a previous study, the parameter X was set to 4 [18].

In addition, the CBC corrects the deterioration of spatial resolution by installing a correction term to OSEM. The correction term considers the blurring of the image caused by the collimator [1]. Therefore, the point-spread function (PSF), representing the response of an imaging system to a point source, is a Gaussian function. The relationship between the full-width-half-maximum (FWHM) of PSF and the source-to-collimator distance is simplified as follows:

$$FWHM = Ax + B \quad [2]$$

where x is the source-to-collimator distance, and A and B are the specific constants for each collimator. Coefficient A indicates the spread per unit distance or the degree of point-spread.

Coefficients A and B are essential to apply 3D-resolution correctio ns. To obtain the data, we simulated the blurring of the image using planar images of point source on each collimator using the HEXAGON and NAI. The geometric arrangement of point-source imaging is illustrated in (Figure 3). The size of the point source of ^{123}I was 1 mm × 1 mm × 1 mm, and the distances between the source and collimator were 100, 200, and 300 mm. Coefficients A and B were used as the correction factors of CBC or the Metz filter (3D-FDR) for each collimator in the Prominence Processor software.

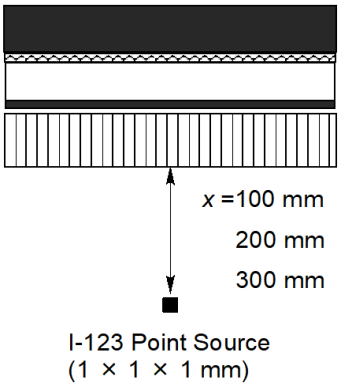

Figure 3: Setup for the simulation of I-123 point source. Here, "x" denotes the distance between the source and collimator.

In this study, five reconstruction methods were assessed: 1. OSEM with AC and SC ("OSEM"); 2. OSEM with AC, SC, and CBC ("OSEM-CBC"); 3. OSEM with AC, SC, and 3D-FDR ("OSEM-FDR"); 4. FBP with AC and SC ("FBP"); and 5. FBP with AC, SC, and 3D-FDR ("FBP-FDR").

V Image Assessment

The reconstructed images were assessed using the specific binding ratio (SBR) of the striatum and the recovery coefficient (RC) of the striatum. SBR is defined as the ratio of the specific binding concentration of the striatum to the background (nonspecific)binding concentration of the whole brain other than the striatum.
SBR is formulated as follows:

$$SBR = \frac{H - B}{B} = \frac{H}{B} - 1 \quad [3]$$

where H denotes the radioactivity concentration of striatum, and B is that of the background. The radioactivity concentration of the right and left striatum was 44.9 and 22.4 kBq/mL, respectively. The concentration of the background was 7.44 or 5.56 kBq/mL. Therefore, the true SBRs were 5.03 and 2.01 or 7.04 and 3.03.

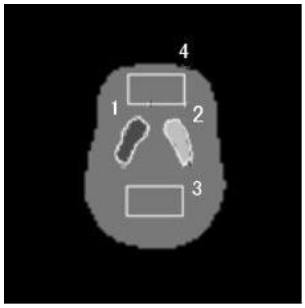

Figure 4: Setting of regions of interest (ROI). **1)** the right striatum, **2)** the left striatum, **3)** the occipital lobe, **4)** the frontal lobe.

The simulated SBR, $SBR_{simulated}$, was calculated from the mean count in the regions of interest (ROIs), as shown in (Figure 4). The background

count included the mean counts of frontal and occipital lobes. RC is defined as the ratio of $SBR_{simulated}$ to SBR_{true}.

$$RC\ [\%] = \frac{SBR_{simulated}}{SBR_{true}} \times 100 \qquad [4]$$

RC indicates the accuracy of the SPECT image.

ROIs are illustrated in (Figure 4). ROIs of the right striatum, left striatum, and whole brain were decided by extracting the contour manually based on the CT image of the striatal phantom. ROIs of frontal and occipital lobes were found to be rectangular. The Prominence Processor software calculated the mean count and standard deviation within these ROIs. In this study, the SPECT images without resolution correction were simulated for all collimators; and then the collimators with RC of >65% were selected and assessed.

Table 2: Coefficient *A* and *B* in Eq. [2] and recovery coefficient (RC) of SPECT images for OSEM without spatial resolution correction.

Collimator	*A*	*B* (mm)	*RC* (%)
LEHR-1	0.047	2.5	64.3
LEHR-2	0.039	3.3	66.3
LEHR-3	0.044	2.8	65.7
LEHR-4	0.041	3.5	67.5
LEHR-5	0.036	3.2	69.0
LEHR-6	0.054	2.7	65.1
LEGP-1	0.043	3.4	61.9
LEGP-2	0.056	3.4	61.0
LEGP-3	0.057	4.4	55.0
LEGP-4	0.062	5.1	51.3
LEGP-5	0.071	5.2	46.9
MEGP-1	0.042	3.8	63.8
MEGP-2	0.047	3.6	66.7
MEGP-3	0.069	2.3	61.3

Results

Table 2 shows the coefficients *A* and *B* presented in equation [2] for 14 collimators and the RC of SPECT images for OSEM without spatial resolution correction. The coefficient *A* indicates the degree of point-spread for the collimator, and the values of high-resolution collimators with high aspect ratio were less than 0.05. (Figure 5A) shows the relationship between *A* and aspect ratio. The *A* was inversely proportional to the aspect ratio. The RC value was the highest with the LEHR-5 collimator, which had the smallest *A*. (Figure 5B) shows the relationship between *A* and RC. Notably, a collimator with small *A* demonstrated high RC.

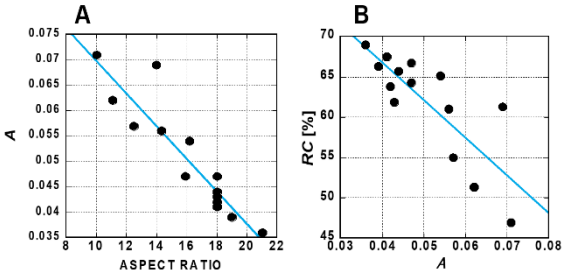

Figure 5: Scatter plot between **A)** coefficient *A* in Eq. [2] for 14 collimators and aspect ratio, **B)** recovery coefficients (RC) and coefficient *A*. Coefficient *A* presents the spread per unit distance.

Figure 6 shows the simulated DaT-SPECT images using the three selected collimators with RC >65%, and (Table 3) and (Figure 7) show the RC with resolution corrections and reconstruction methods. Most collimators were LEHR with the high aspect ratio, and the RC increased by 1.1-1.2 times with resolution correction. In terms of the reconstruction method, the values obtained using OSEM were insignificantly higher than those obtained using FBP. Furthermore, CBC was more effective than FDR (Metz filter). RC using the LEHR-5 collimator was the highest in all cases. The difference in RC between collimators decreased with resolution correction.

Figure 6: Simulated SPECT images for each image reconstruction method for three collimators. The concentrations of background, the right striatum, and the left striatum were 5.58, 44.9, and22.4 kBq/mL, respectively.

Table 3: Recovery coefficient RC (%) of SPECT images for each image reconstruction method for selected 6 collimators.

	Collimator					
	LEHR-2	LEHR-3	LEHR-4	LEHR-5	LEHR-6	MEGP-2
OSEM	66.3	65.7	67.5	69.0	65.1	66.7
OSEM-CBC	77.7	78.5	79.4	79.7	78.3	76.5
OSEM-FDR	77.1	77.9	78.9	78.7	77.9	75.3
FBP	65.6	66.4	66.8	68.1	64.9	63.3
FBP-FDR	75.6	77.5	77.6	77.9	76.7	73.8

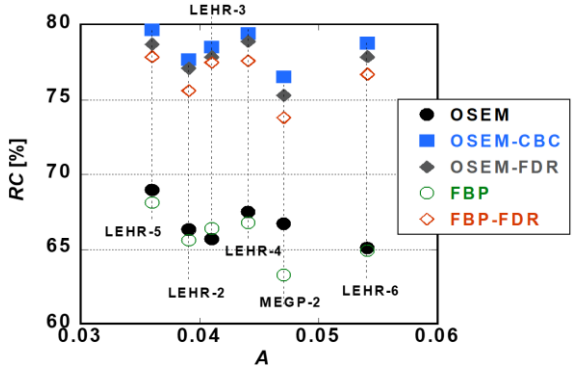

Figure 7: Scatter plot between recovery coefficient (RC) and coefficient *A* presented in Eq. [2] for 6 selected collimators. Plots on vertical dashed line denote the data for the same collimator.

Discussion

The primary factor that controls the quality of the SPECT image is the performance of the collimators. Collimators with low spatial resolution blur the outline of the hot area, and the concentration distribution spills out of ROI. Therefore, the count number in ROI decreases, resulting in a decreased RC. The high-resolution collimators showed high aspect ratios, as shown in (Table 1), and efficiently blocked the photons that did not incident vertically to the collimator and demonstrated higher spatial resolution and higher RC. On the contrary, the collimators with low aspect ratios (for example, LEGP-5 in Table 1) demonstrated low RC because of the blurring of the hot area, despite the increased sensitivity due to the large hole diameter (0.178 - 0.254 cm). Collimators with a thin septum, such as LEGP-1, demonstrated lower RC due to the blur caused by the penetration photons, although the aspect ratio was high.

In this study, the collimator performance for spatial resolution was quantified using coefficient *A* in the equation (2). The coefficient *A* indicates the degree of point-spread; therefore, collimators with low *A* demonstrated higher RC. The LEHR-5 collimator had the lowest *A* in this study, demonstrating the highest RC. The six selected collimators were almost LEHR, with low *A*. The MEGP-2 collimator had a thick septum (0.066 cm) that blocked penetration or oblique photons and resulting in high RC.

Spatial resolution correction improved the RC by approximately 20 %. The resolution correction sharpened the profile of the striatum and decreased the spill-out of ROI, and thus increased RC. However, the resolution correction did not change the relative magnitude correlation between RCs produced by collimators; the LEHR-5 collimator demonstrated the highest RC. However, the difference in RC between collimators was decreased. In terms of the correction method, the effect of CBC was like that of the FDR.

Results are of course, dependent on the type of filter. The only filter available for this study was the Metz filter, due to the fact that it is the only installed filter in the Prominence Processor software package. In addition, we adopted ^{123}I as a nuclide; therefore, the obtained information in this study is limited to the photon energy of about 159 keV dependent on the kind of nuclide (photon energy).

Conclusion

In this study, we simulated I-123 DaT-SPECT images in presence of various conditions to assess the impact of collimator using Monte Carlo simulation in which a digitized striatum phantom was installed. The collimators with high aspect ratio demonstrated better quality in SPECT imaging. The spatial resolution correction improved the RC by approximately 20%. The resolution correction did not change the relative magnitude correlation between RCs produced by collimators; however, the difference in the recovery coefficients between collimators was decreased. Consequently, the LEHR collimator with a high aspect ratio and OSEM with spatial resolution correction were confirmed to be appropriate with respect to DaT-SPECT.

Conflicts of Interest

None.

References

1. Yokoi T, Shinohara H, Ohnishi H (2002) Performance evaluation of OSEM reconstruction algorithm incorporating three-dimensional distance-dependent resolution compensation for brain SPECT: A simulation study. *Ann Nucl Med* 16: 11-18. [Crossref]
2. Maebatake A, Imamura A, Kodera Y et al. (2016) Evaluation of iterative reconstruction method and attenuation correction in brain dopamine transporter SPECT using an anthropomorphic striatal phantom. *Asia Oceania J Nucl Med Biol* 4: 72-80. [Crossref]
3. Booij J, Speelman JD, Martin Horstink WIM, Wolters EC (2001) The clinical benefit of imaging striatal dopamine transporters with ^{123}IFPCIT SPET in differentiating patients with presynaptic parkinsonism from those with other forms of parkinsonism. *Eur J Nucl Med* 28: 266-272. [Crossref]
4. Booij J, Tissingh G, Boer GJ, Speelman JD, Stoof JC et al. (1997) ^{123}I FP-CIT SPECT shows a pronounced decline of striatal dopamine transporter labelling in early and advanced Parkinson's disease. J *Neurol Neurosurg Psychiatry* 62: 133-140. [Crossref]

5. Benamer HTS, Patterson J, Grosset DG, et al. (2000) Accurate differentiation of Parkinsonism and essential tremor using visual assessment of ^{123}I -FP-CIT SPECT imaging: The ^{123}I -FP-CIT study group. *Mov Disord* 15: 503-510.
6. Darcourt J, Booij J, Tatsch K, Varrone A, Borght TV et al. (2010) EANM procedure guidelines for brain neurotransmission SPECT using ^{123}I -labelled dopamine transporter ligands, version2. *Eur J Nucl Med Mol Imaging* 37: 443-50.
7. Dickson JC, Tossici-Bolt L, Sera T, Erlandsson K, Varrone A et al. (2010) The impact of reconstruction method on the quantification of DaTSCAN images. *Eur J Nucl Med Mol Imaging* 37: 23-35. [Crossref]
8. Römer W, Reichel N, Vija HA, Nickel I, Hornegger J et al. (2006) Isotropic reconstruction of SPECT data using OSEM3D: correlation with CT1. *Acad Radiol* 13: 496-502. [Crossref]
9. Kohli V, King MA, Glick SJ, Pan T-S (1998) Comparison of frequency-distance relationship and Gaussian-diffusion-based methods of compensation for distance-dependent spatial resolution in SPECT imaging. *Phys Med Biol* 43: 1025-1037. [Crossref]
10. Xia W, Lewitt R M, Edholm P R (1995) Fourier correction for spatially variant collimator blurring in SPECT. *IEEE Trans Med Img* 14: 100-115.
11. Ogawa K, Katsu H (1996) Iterative correction method for shift-variant blurring caused by collimator aperture in SPECT. *Ann Nucl Med* 10: 33-40. [Crossref]
12. Uehara S (1986) The development of a Monte Carlo code simulating electron-photon showers and its evaluation by various transport benchmarks. *Nucl Insrum Methods Phys Res B* 14: 559-570.
13. Takahashi A, Himuro K, Yamashita Y, Komiya I, Baba S et al. (2015) Monte Carlo simulation of PET and SPECT imaging of ^{90}Y. *Med Phys* 42: 1926-1935. [Crossref]
14. Tanaka M, Uehara S, Kojima A, Matsumoto M (2007) Monte Carlo simulation of energy spectra for ^{123}I imaging. *Phys Med Biol* 52: 4409-4425. [Crossref]
15. Djang DSW, Janssen MJR, Bohnen N, et al. (2012) SNM practice guideline for dopamine transporter imaging with ^{123}I -Ioflupane SPECT 1.0. *J Nucl Med* 53: 154-163.
16. Ioflupane Lupine Guidelines Working Group (2017) Ioflupane clinical practice guidelines, second edition (in Japanese). *Japanese Society of Nuclear Medicine and the Japanese Council of Nuclear Neuroimaging*.
17. Matsumoto N, Nagaki A, Yamao F, Sasaki M (2015) Optimization of iterative reconstruction parameters with 3–dimensional resolution recovery, scatter and attenuation correction in ^{123}I-FP-CIT SPECT. *Ann Nucl Med* 29: 636-642.
18. Gilland DR, Tsui BMW, McCartney WH, Perry JR, Jan Berg J (1988) Determination of the optimum filter function for SPECT imaging. *J Nucl Med* 29: 643-650. [Crossref]